Journal of Knot Theory and Its Ramifications Vol. 16, No. 5 (2007) 545–574

STRUCTURES OF SMALL CLOSED NON-ORIENTABLE 3-MANIFOLD TRIANGULATIONS

BENJAMIN A. BURTON
School of Mathematical and Geospatial Sciences, RMIT University
GPO Box 2476V, Melbourne VIC 3001, Australia
bab@debian.org

ABSTRACT

A census is presented of all closed non-orientable 3-manifold triangulations formed from at most seven tetrahedra satisfying the additional constraints of minimality and $\mathbb{P}^2$-irreducibility. The eight different 3-manifolds represented by these 41 different triangulations are identified and described in detail, with particular attention paid to the recurring combinatorial structures that are shared amongst the different triangulations. Using these recurring structures, the resulting triangulations are generalised to infinite families that allow similar triangulations of additional 3-manifolds to be formed.

Keywords: 3-manifold; minimal triangulation; census.

1. Introduction

It is useful when studying 3-manifold topology to have a complete reference of all 3-manifold triangulations satisfying some broad set of constraints. Examples include Callahan, Hildebrand and Weeks' census of cusped hyperbolic 3-manifold triangulations formed from at most seven tetrahedra [7] and Matveev's census of closed orientable triangulations formed from at most six tetrahedra [15].

Such references provide an excellent pool of examples for testing hypotheses and searching for triangulations that satisfy unusual properties. In addition they offer insight into the structures of minimal 3-manifold triangulations. In fact, since very few sufficient conditions for minimality are currently known, censuses play an important role in proving the minimality of small triangulations.

Much recent progress has been made in enumerating closed orientable 3-manifolds and their triangulations. Matveev presents a census of closed orientable triangulations formed from at most six tetrahedra [15], extended to seven tetrahedra by Ovchinnikov. Martelli and Petronio form a census of closed orientable 3-manifolds formed from up to nine tetrahedra [13], although they are primarily concerned with

the 3-manifolds and their geometric structures and so the triangulations themselves are not listed. More recently their census has been extended to ten tetrahedra by Martelli [12].

Less progress has been made regarding closed non-orientable triangulations. Amendola and Martelli present a census of closed non-orientable 3-manifolds formed from up to six tetrahedra [1], a particularly interesting census because it is constructed without the assistance of a computer. Again these authors are primarily concerned with the 3-manifolds and their geometric structures, and so not all triangulations of these 3-manifolds are obtained.

Here we extend the closed non-orientable census of Amendola and Martelli to seven tetrahedra, and in addition we enumerate the many different triangulations of these 3-manifolds instead of just the 3-manifolds themselves. Furthermore we examine the combinatorial structures of these triangulations in detail, highlighting common constructions that recur throughout the census triangulations.

Independently of this work, Amendola and Martelli have also announced an extension of their non-orientable census to seven tetrahedra [2]. As in their six-tetrahedron census they concentrate only on the resulting 3-manifolds and not their different triangulations, but again the non-computational nature of their work is remarkable.

As with the previous closed censuses described above, we consider only triangulations satisfying the following constraints.

- *Closed:* The triangulation is of a closed 3-manifold. In particular it has no boundary faces, and each vertex link is a 2-sphere.
- $\mathbb{P}^2$*-irreducible:* The underlying 3-manifold has no embedded two-sided projective planes, and furthermore every embedded 2-sphere bounds a ball.
- *Minimal:* The underlying 3-manifold cannot be triangulated using strictly fewer tetrahedra.

Requiring triangulations to be $\mathbb{P}^2$-irreducible and minimal keeps the number of triangulations down to manageable levels, focussing only upon the simplest triangulations of the simplest 3-manifolds (from which more complex 3-manifolds can be constructed). Minimal triangulations prove to be particularly useful for studying the 3-manifolds that they represent, since they are frequently well structured as seen in both Matveev's census [15] and the results presented here.

For the $\leq$ 7-tetrahedron non-orientable census presented in this paper, a brief summary of results is presented in Table 1. Each triangulation is counted once up to isomorphism, i.e., a relabelling of the tetrahedra within the triangulation and their individual faces. It is worth noting that the number of triangulations is significantly larger than the number of 3-manifolds, since most 3-manifolds in the census can be realised by several different minimal triangulations.

The final 41 triangulations are found to be remarkably similar in their construction. By identifying these similarities we construct a small handful of infinite

Table 1. Summary of closed non-orientable census results

Tetrahedra	**3-Manifolds**	**Triangulations**
≤ 5	0	0
6	5	24
7	3	17
Total	8	41

parameterised families of 3-manifold triangulations that encompass 38 of these 41 triangulations. The remaining three triangulations are all six-tetrahedron triangulations and might well be small exceptional cases that do not generalise at all — an extension of this census to higher numbers of tetrahedra should offer further insight.

We do not discuss here the algorithms used in constructing the census. The generation of triangulations follows the basic framework described by Hildebrand and Weeks [9] and used by many authors since, involving the enumeration of tetrahedron face pairings and then the selection of individual gluing permutations for each pair of faces. Several recent results are used to reduce the heavy computational load, including in particular the face pairing constraints and other non-orientable structural results of [5]. The subsequent analysis of triangulations draws on many techniques, including Pachner moves [16] and other localised transformations, normal surface analysis, homology calculations, and the very useful Turaev-Viro invariants [17].

The remainder of this paper is devoted to presenting the census results and describing in detail the combinatorial structures of the various triangulations. Section 2 describes the construction of thin I-bundles and layered solid tori, which are parameterised building blocks that recur frequently throughout the census triangulations. In Section 3 we combine these building blocks to form our infinite families of 3-manifold triangulations, as well as describing the three exceptional triangulations from the census that these families do not cover. Finally Section 4 closes with a full listing of the 41 triangulations found in the census, using the constructions of Sections 2 and 3 to simplify their descriptions and identify the underlying 3-manifolds.

All of the computational work was performed using *Regina*, a computer program that performs a variety of different calculations and procedures in 3-manifold topology [3, 6]. The program *Regina*, its source code and accompanying documentation are freely available from `http://regina.sourceforge.net/`.

Special thanks must go to J. Hyam Rubinstein for many helpful discussions throughout the course of this research.

2. Common Structures

In order to make the census triangulations easier to both visualise and analyse, we decompose these triangulations into a variety of building blocks. Ideally such building blocks should be large enough that they significantly simplify the repre-

sentation and analysis of the triangulations containing them, yet small enough that they can be frequently reused throughout the census.

This idea of describing triangulations using medium-sized building blocks has been used previously for the orientable case. Matveev describes a few orientable building blocks [15] and Martelli and Petronio describe a more numerous set of smaller orientable building blocks called *bricks* [13].

An examination of the non-orientable triangulations of this census shows a remarkable consistency of combinatorial structure. We therefore need only two types of building block: the thin I-bundle and the layered solid torus.

2.1. *Thin I-Bundles*

A thin I-bundle is essentially a triangulation of an I-bundle over some surface S that has a thickness of only one tetrahedron between its two parallel boundaries. Thin I-bundles play an important role in the construction of minimal non-orientable triangulations and appear within all of the triangulations in this census.

An important feature of a thin I-bundle is a copy of the surface S that runs through its centre; this surface is broken down by the individual tetrahedra into triangles and quadrilaterals. It will be seen that this decomposition of S is in fact sufficient to completely reconstruct the thin I-bundle.

The advantage of working with this decomposition of S is that surfaces are generally easier to visualise and analyse than entire 3-manifold triangulations. We therefore use triangle and quadrilateral decompositions of surfaces as a starting point for defining thin I-bundles, and also as a preferred method of representing them pictorially.

We begin this section by describing constraints that such a surface decomposition must satisfy. Following this we show how a surface decomposition can be fleshed out to form a 3-manifold triangulation, from which we formally define a thin I-bundle in Definition 2.6. Finally we discuss pictorial representations, and how markings can be added to a surface decomposition to show how the resulting I-bundle is twisted, if at all.

Definition 2.1 (Well-Balanced Decomposition) Let S be some closed surface. A *well-balanced decomposition* of S is a decomposition of S into triangles and quadrilaterals satisfying the following properties.

1. Every vertex of the decomposition meets an even number of quadrilateral corners.

2. If the quadrilaterals are removed then the surface breaks into a disconnected collection of triangulated discs. Here "disconnected" means that the discs may touch at vertices but not along edges, as illustrated in Figure 1.

3. There are no cycles of quadrilaterals. That is, any path formed by walking through a series of quadrilaterals, always entering and exiting by opposite

sides, must eventually run into a triangle.

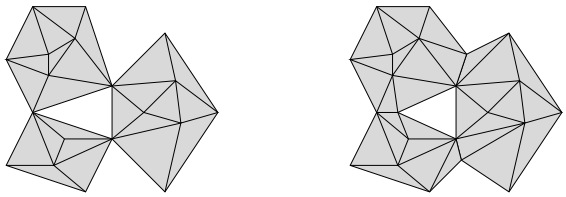

Fig. 1. Forming a disconnected collection of triangulated discs

To clarify condition 3, Figure 2 illustrates some arrangements of quadrilaterals that contain cycles as described above. In each diagram the offending cycle is marked by a dotted line. Figure 3 on the other hand illustrates arrangements of quadrilaterals that do not contain cycles and so are perfectly acceptable within a well-balanced decomposition.

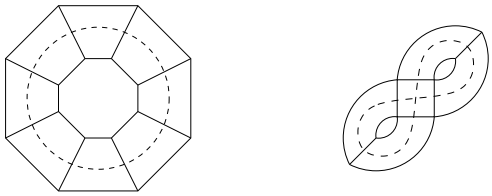

Fig. 2. Arrangements of quadrilaterals that include cycles

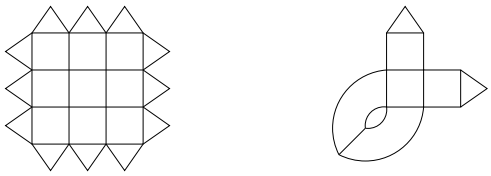

Fig. 3. Arrangements of quadrilaterals that do not include cycles

Example 2.2 Figure 4 illustrates a handful of well-balanced decompositions of the torus. Each of these decompositions can be seen to satisfy all of the conditions of Definition 2.1.

Figure 5 however illustrates some decompositions of the torus that are not well-balanced. The first diagram illustrates a decomposition that breaks condition 1

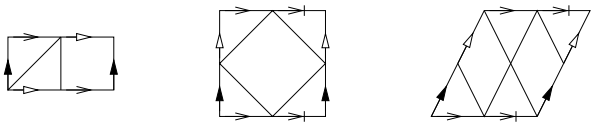

Fig. 4. Well-balanced decompositions of the torus

of Definition 2.1; one of the offending vertices is marked with a black circle. The second diagram shows how this same decomposition breaks condition 3; two cycles of quadrilaterals are marked with dotted lines. The final decomposition breaks condition 2 (amongst others); the shaded triangles together form an annulus, not a disc.

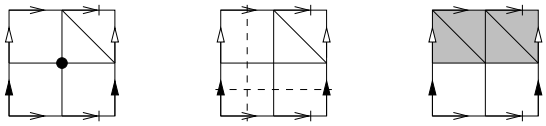

Fig. 5. Decompositions of the torus that are not well-balanced

Once we have obtained a well-balanced decomposition of a surface, we can flesh out its triangles and quadrilaterals into a full 3-manifold triangulation as seen in the following definition.

Definition 2.3 (Enclosing Triangulation) Let D be a well-balanced decomposition of a closed surface. The *enclosing triangulation* of D is the unique 3-manifold triangulation formed as follows.

Each triangle or quadrilateral of D is enclosed within its own tetrahedron as illustrated in Figure 6. The faces of these tetrahedra are then identified in the unique manner that causes these discs to be connected according to the decomposition D. Any tetrahedron faces that do not meet any discs of D (i.e., the faces parallel to triangular discs) become boundary faces of the enclosing triangulation.

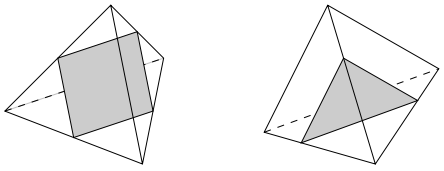

Fig. 6. Enclosing triangles and quadrilaterals within tetrahedra

Example 2.4 To illustrate the joining of two tetrahedra, Figure 7 shows quadrilaterals q and q' placed within tetrahedra Δ and Δ' respectively. Suppose that edges e and e' of these quadrilaterals are identified within the surface decomposition D. Then tetrahedron faces f and f' must be identified as illustrated so that edges e and e' can be connected correctly.

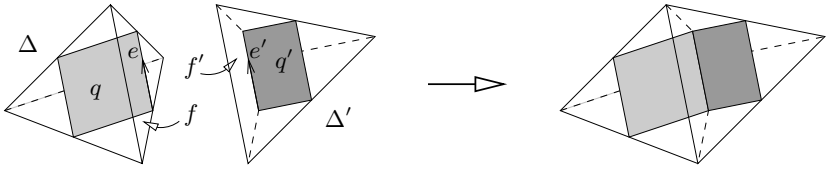

Fig. 7. Joining two tetrahedra in the enclosing triangulation

For a larger example, consider the well-balanced decomposition of the torus depicted in the left hand diagram of Figure 8. The enclosing triangulation of this decomposition is illustrated to its right, where the six discs have become six tetrahedra.

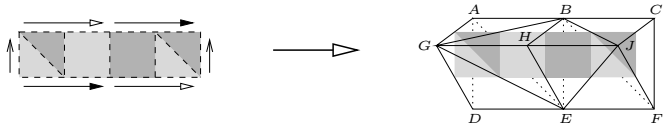

Fig. 8. Constructing an entire enclosing triangulation

As mandated by the torus decomposition, we identify the following pairs of faces:

$$ADG \leftrightarrow CFJ, \qquad ABG \leftrightarrow HJE, \qquad BCJ \leftrightarrow GHE,$$
$$BGH \leftrightarrow JEF, \qquad BHJ \leftrightarrow GDE.$$

Note that the final four identifications in this list put a twist in the I-bundle, so that the enclosing triangulation is of a twisted I-bundle over the torus. The rear faces ABE, ADE, BCF and BEF remain boundary faces of the enclosing triangulation.

Since each disc of the surface decomposition D runs through the centre of a tetrahedron, we see that the enclosing triangulation essentially "thickens" the surface decomposition D into a 3-dimensional triangulation (as formalised in the lemma below). The original surface with its triangles and quadrilaterals in turn becomes a normal surface running through the centre of the enclosing triangulation.

Lemma 2.5 Let D be a well-balanced decomposition of the closed surface S. Then the enclosing triangulation of D is a 3-manifold triangulation representing an I-bundle (possibly twisted) over S.

Proof Let T be the enclosing triangulation. Our first step is to prove that T is in fact a triangulation of a 3-manifold.

It can be shown that each edge not meeting the central decomposition D is in fact a boundary edge of the triangulation. This is clearly true of edges belonging to tetrahedra that enclose triangles of D, since faces parallel to triangles of D become boundary faces of the overall triangulation. This is also true of edges belonging to tetrahedra that enclose quadrilaterals of D, since condition 3 of Definition 2.1 (no cycles of quadrilaterals) ensures that each such edge is identified with an edge of one of the boundary faces previously described.

Each internal edge of T therefore cuts through a vertex of the decomposition D. Condition 1 of Definition 2.1 (vertices meet an even number of quadrilateral corners) ensures that no internal edge of T is identified with itself in reverse.

We turn now to the vertices of T. By observing how the tetrahedra are hooked together we see that the link of each vertex v is of the form illustrated in Figure 9.

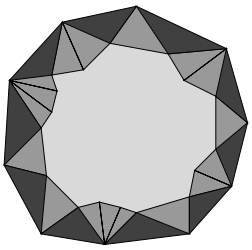

Fig. 9. A vertex link in an enclosing triangulation

The dark shaded triangles around the outside correspond to tetrahedra enclosing triangles of D in which v belongs to a boundary face. This is illustrated in the left hand diagram of Figure 10. These dark shaded triangles provide the boundary edges of the vertex link.

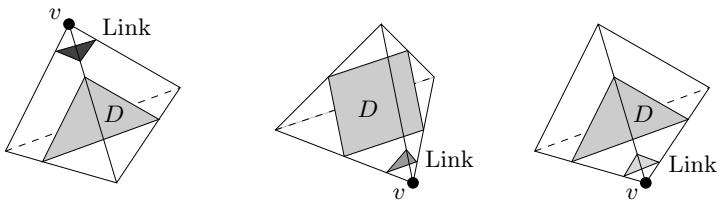

Fig. 10. Pieces of a vertex link

The medium shaded triangles just inside this boundary correspond to tetrahedra enclosing quadrilaterals of D, as illustrated in the central diagram of Figure 10. Each of these medium shaded triangles meets the boundary at a single point, since

we observed earlier that each edge of T running parallel to a quadrilateral of D is in fact a boundary edge.

The remaining pieces of the vertex link, corresponding to the light shaded region in the interior of Figure 9, are provided by tetrahedra enclosing triangles of D in which v lies opposite the boundary face. In these cases the pieces of the vertex link run parallel to the triangles of D as illustrated in the right hand diagram of Figure 10. From condition 2 of Definition 2.1 (triangulated regions form discs in D) we see that these interior pieces combine to form a topological disc. Thus v is a boundary vertex (i.e., the darker band forming the boundary of Figure 9 actually exists), and more importantly the entire link of vertex v is a topological disc.

Thus our enclosing triangulation T is indeed a triangulation of a 3-manifold. From the fact that the well-balanced decomposition of the surface S runs through the centre of each tetrahedron, as well as the earlier observation that each vertex, edge and face not meeting this surface decomposition in fact forms part of the triangulation boundary, it is straightforward to see that the enclosing triangulation represents an I-bundle (possibly twisted) over S. □

Definition 2.6 (Thin I-Bundle) A *thin I-bundle* over a closed surface S is the enclosing triangulation of a well-balanced decomposition of S. This well-balanced decomposition is referred to as the *central surface decomposition* of the thin I-bundle.

We see then that Lemma 2.5 simply states that a thin I-bundle over a surface S is what it claims to be, i.e., an actual triangulation of an I-bundle over S.

Before closing this section we present a method of marking a well-balanced decomposition that allows us to establish precisely how the corresponding I-bundle is twisted, if at all.

Definition 2.7 (Marked Decomposition) A well-balanced decomposition can be *marked* to illustrate how it is embedded within its enclosing triangulation. Markings consist of solid lines and dotted lines, representing features above and below the central surface respectively.

The different types of markings are illustrated in Figure 11. Each quadrilateral lies between two perpendicular boundary edges of the triangulation, one above and one below. These boundary edges are represented by a solid line and a dotted line as illustrated in the left hand diagram of Figure 11. Each triangle lies between a boundary vertex and a boundary face. If the boundary vertex lies above the triangle (and the boundary face below) then the triangle is marked with three solid lines as illustrated in the central diagram of Figure 11. If the boundary vertex lies below the triangle (and the boundary face above) then the triangle is marked with three dotted lines as illustrated in the right hand diagram.

Since the edges and vertices of the I-bundle boundary all connect together, it follows that the markings must similarly connect together, with solid lines matched

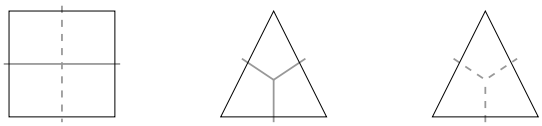

Fig. 11. Marking quadrilaterals and triangles

with solid lines and dotted lines matched with dotted lines. Following these markings across edge identifications therefore allows us to see if and where a region above the central surface moves through a twist to become a region below.

Example 2.8 Figure 12 illustrates three well-balanced decompositions of the torus with markings. In the first diagram we see that the I-bundle is twisted across the upper and lower edge identifications, since solid lines change to dotted lines across these identifications and vice versa. There is no twist however across the left and right edge identifications since the solid line does not change.

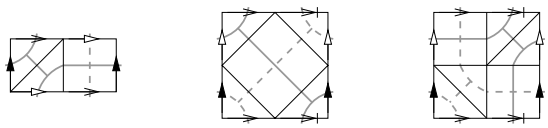

Fig. 12. Markings on well-balanced torus decompositions

In the second diagram we see that the I-bundle is twisted across all of the outer edge identifications, with solid and dotted lines being exchanged in every case. In the third diagram we see that there are no twists at all, and that the I-bundle is simply the product $T^2 \times I$.

2.2. *Layered Solid Tori*

A key structure that appears frequently within both orientable and non-orientable minimal triangulations is the layered solid torus. Layered solid tori have been discussed in a variety of informal contexts by Jaco and Rubinstein. They appear in [10] and are treated thoroughly in [11]. Analogous constructs involving special spines of 3-manifolds can be found in [14] and [15]. The preliminary definitions presented here follow those given in [5].

In order to describe the construction of a layered solid torus we introduce the process of layering. Layering is a transformation that, when applied to a triangulation with boundary, does not change the underlying 3-manifold but does change the curves formed by the boundary edges of the triangulation.

Definition 2.9 (Layering) Let T be a triangulation with boundary and let e be one of its boundary edges. To *layer a tetrahedron on edge* e, or just to *layer on edge* e, is to take a new tetrahedron Δ, choose two of its faces and identify them with the two boundary faces on either side of e without twists. This procedure is illustrated in Figure 13.

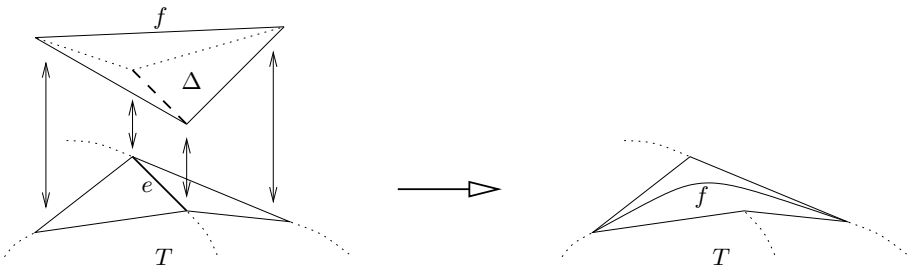

Fig. 13. Layering a tetrahedron on a boundary edge

Note that layering on a boundary edge does not change the underlying 3-manifold; the only effect is to thicken the boundary around edge e. Moreover, once a layering has been performed, edge e is no longer a boundary edge but instead edge f (which in general represents a different curve on the boundary of the 3-manifold) has been added as a new boundary edge.

Definition 2.10 (Layered Solid Torus) A *standard layered solid torus* is a triangulation of a solid torus formed as follows. We begin with the one-triangle Möbius band illustrated in the left hand diagram of Figure 14, where the two edges marked e are identified according to the arrows and where g is a boundary edge. This Möbius band can be embedded in $\mathbb{R}^3$ as illustrated in the right hand diagram of Figure 14.

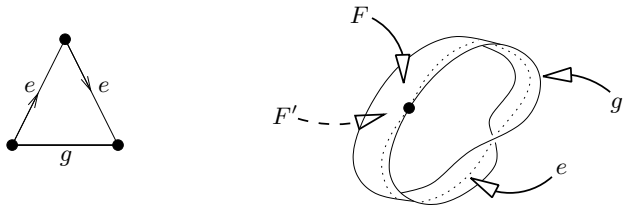

Fig. 14. A one-triangle Möbius band

In this embedding our single triangular face has two sides, marked F and F' in the diagram. We make an initial layering upon edge e as illustrated in Figure 15, so that faces ABC and BCD of the new tetrahedron are joined to sides F and F'

respectively of the original triangular face. Although the initial Möbius band is not actually a 3-manifold triangulation, the layering procedure remains the same as described in Definition 2.9.

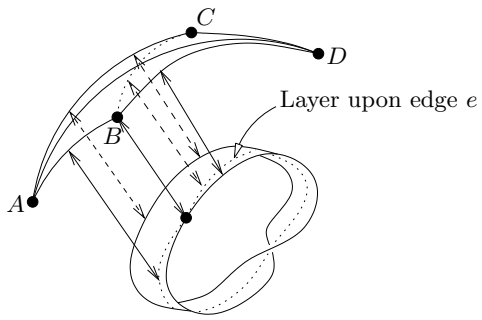

Fig. 15. Layering on a Möbius band to form a solid torus

Since F and F' are in fact opposite sides of the same triangular face, we see that faces ABC and BCD become identified to give us the well-known one-tetrahedron triangulation of the solid torus with two boundary faces.

Having obtained a real 3-manifold triangulation of the solid torus, we finish the construction by performing some number of additional layerings upon boundary edges, one at a time. We may layer as many times we like or we may make no additional layerings at all. There are thus infinitely many different standard layered solid tori that can be constructed.

The Möbius band on its own can be considered as a *degenerate layered solid torus* containing zero tetrahedra; this will prove useful to us in later sections.

We can observe that each standard layered solid torus has two boundary faces and represents the same underlying 3-manifold, i.e., the solid torus. What distinguishes the different layered solid tori is the different patterns of curves that their boundary edges make upon the boundary torus.

Definition 2.11 (Layered Solid Torus Parameters) Let L be a layered solid torus. Arbitrarily label the two boundary faces $+$ and $-$, and draw a meridinal curve in general position on this boundary. Assign an arbitrary orientation to this meridinal curve, and arbitrarily label the three boundary edges e_1, e_2 and e_3.

Define *intersection numbers* k_1, k_2 and k_3, where k_i is the number of times the meridinal curve crosses edge e_i from $+$ to $-$ minus the number of times it crosses edge e_i from $-$ to $+$. Then L is said to be a (k_1, k_2, k_3) *layered solid torus*, denoted $\mathrm{LST}(k_1, k_2, k_3)$.

An example of this can be seen in Figure 16. In this case the intersection numbers are $k_1 = 2$, $k_2 = 3$ and $k_3 = -5$, giving us a $(2, 3, -5)$ layered solid torus.

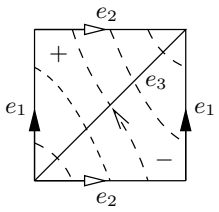

Fig. 16. The meridinal curve on the boundary of a $(2, 3, -5)$ layered solid torus

It can be shown that these intersection numbers are well-defined, and that for any $\mathrm{LST}(p, q, r)$ we have $p + q + r = 0$ with p, q, r pairwise coprime. From the arbitrary decisions made in Definition 2.11 it is clear that a (p, q, r) layered solid torus is also a $(-p, -q, -r)$ layered solid torus, and that the parameters may be reordered at will (so for instance a (p, q, r) layered solid torus is also a (p, r, q) or a (q, r, p) layered solid torus).

Example 2.12 A $(1, 2, -3)$ layered solid torus formed from one tetrahedron is illustrated in Figure 17. This is the one-tetrahedron solid torus described in Definition 2.10, formed by a single layering upon the original Möbius band.

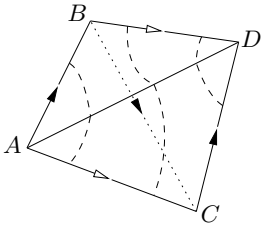

Fig. 17. A $(1, 2, -3)$ layered solid torus

The two rear faces ABC and BCD of the tetrahedron are identified, and the two front faces ABD and ACD form the boundary torus. A meridinal curve on this boundary is illustrated by the dashed line in the diagram; note that this curve meets the three boundary edges in one, two and three points respectively.

Example 2.13 The degenerate layered solid torus with zero tetrahedra, i.e., the Möbius band, can be considered as a $(1, 1, -2)$ layered solid torus. Recall how the Möbius band was embedded in $\mathbb{R}^3$; here the meridinal curve runs across the top of the strip from boundary to boundary and then back again on the underside of the strip, as illustrated in Figure 18 (think of the strip as slightly thickened).

The three edges of the (degenerate) boundary torus are g and the two sides of

edge e. It can be seen that the meridinal curve meets g twice and each side of edge e once, giving us the parameters $(1, 1, -2)$ as claimed.

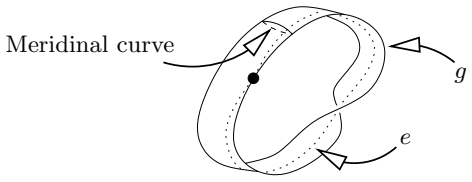

Fig. 18. The degenerate LST$(1, 1, -2)$

Given a set of layered solid torus parameters, it is straightforward to calculate which successive layerings must be performed upon the initial Möbius band to achieve these parameters using as few tetrahedra as possible. The relevant algorithms are described by Matveev [15] and also by Jaco and Rubinstein [11], and we do not reproduce them here. The resulting triangulation is unique up to isomorphism, and any reference to an LST(p, q, r) in the following sections is assumed to refer to the unique minimal layered solid torus with these parameters.

3. Families of Closed Triangulations

Having developed a set of medium-sized building blocks in Section 2, we can now combine these building blocks to form closed triangulations. In this section we present a number of families of closed triangulations, each of which represents an infinite class of triangulations sharing a common large-scale structure. It is seen in Section 4 that, with the exception of the three triangulations described in Section 3.5, the three families presented here together encompass all closed non-orientable minimal $\mathbb{P}^2$-irreducible triangulations formed from up to seven tetrahedra.

A categorisation of triangulations into infinite families as described above is certainly appealing. Large classes of triangulations may be studied simultaneously, and algorithms become available for generating triangulations of infinite classes of 3-manifolds.

Furthermore, when presented with an arbitrary triangulation of an unknown 3-manifold, having a rich collection of such families at our disposal increases the chance that we can identify this 3-manifold. Specifically, if we can manipulate the triangulation into a form that is recognised as a member of one of these families then the underlying 3-manifold can be subsequently established.

In the case of orientable 3-manifolds, several infinite parameterised families of triangulations are described in the literature [4, 13, 14, 15].

3.1. *Notation*

We begin by outlining some notation that is used to describe torus and Klein bottle bundles over the circle.

- $T^2 \times I/A$ represents a torus bundle over the circle, where A is a unimodular 2×2 matrix indicating the homeomorphism under which the torus $T^2 \times \{0\}$ is identified with the torus $T^2 \times \{1\}$. Note that this space is orientable or non-orientable according to whether the determinant of A is $+1$ or -1.

  More specifically, let μ_0 and λ_0 be closed curves that together generate the fundamental group of the first torus and let μ_1 and λ_1 be the curves parallel to these on the second torus. If

  $$A = \begin{bmatrix} a & b \\ c & d \end{bmatrix},$$

  then the homeomorphism under which the two tori are identified maps curve μ_0 to $\mu_1^a \lambda_1^c$ and curve λ_0 to $\mu_1^b \lambda_1^d$.

- $K^2 \times I/A$ represents a Klein bottle bundle over the circle, where A is again a unimodular 2×2 matrix indicating the homeomorphism under which the Klein bottle $K^2 \times \{0\}$ is identified with the Klein bottle $K^2 \times \{1\}$.

  Let μ_0 and λ_0 be orientation-preserving and orientation-reversing closed curves respectively on the first Klein bottle that meet transversely in a single point. It is known that every element of the fundamental group of this Klein bottle can be represented as $\mu^p \lambda^q$ for some unique pair of integers p and q.

  Let μ_1 and λ_1 be the corresponding curves on the second Klein bottle. If

  $$A = \begin{bmatrix} a & b \\ c & d \end{bmatrix},$$

  then the homeomorphism under which the two Klein bottles are identified maps curve μ_0 to $\mu_1^a \lambda_1^c$ and curve λ_0 to $\mu_1^b \lambda_1^d$. It is shown in [8] that every such matrix A must be of the form

  $$A = \begin{bmatrix} \pm 1 & b \\ 0 & \pm 1 \end{bmatrix}.$$

The notation described above is consistent with that used by Matveev for orientable 3-manifolds [15].

3.2. *Layered Surface Bundles*

Our first family of triangulations is the family of layered surface bundles, constructed from untwisted thin I-bundles as follows.

Definition 3.1 (Layered Surface Bundle) A *layered surface bundle* is a specific triangulation of a closed surface bundle over the circle formed using the following construction. We begin with a thin I-bundle over a closed surface S, as described in Definition 2.6. We require this thin I-bundle to have no twists, so that it has two parallel boundary components each representing the same surface S.

We then have the option of layering additional tetrahedra upon these boundary surfaces in order to change the curves formed by the boundary edges; see Definition 2.9 for a detailed description of the layering process. Finally we identify the two boundary surfaces according to some homeomorphism, forming an S-bundle over the circle. An overview of this procedure is illustrated in Figure 19.

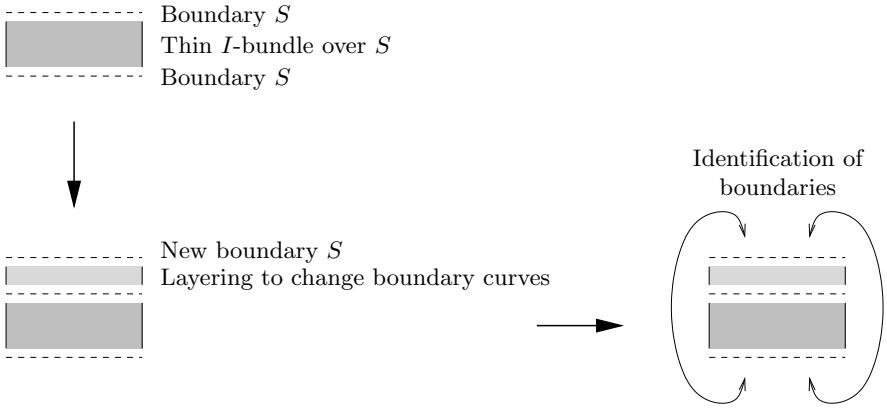

Fig. 19. Constructing a layered surface bundle

We proceed to describe in detail some particular classes of layered surface bundles that feature in the ≤ 7-tetrahedron non-orientable census.

Definition 3.2 In Figure 20 we see pictorial representations of five specific thin I-bundles (the meanings of these diagrams will be explained shortly). In particular, triangulations T_6^1, T_6^2 and T_7 are thin I-bundles over the torus and triangulations K_6^1 and K_6^2 are thin I-bundles over the Klein bottle. Each of these I-bundles is untwisted, with two parallel boundary components each formed from two triangles.

The left hand portion of each diagram depicts the central surface decomposition of the thin I-bundle, complete with markings as described in Definition 2.7. The right hand portion illustrates the upper and lower boundary components of the enclosing triangulation, marked in solid lines and dotted lines respectively. Figure 21 shows in more detail how the two portions of the diagram relate for the case T_6^2.

For each thin I-bundle we mark directed edges α_1 and β_1 on the upper boundary component and α_2 and β_2 on the lower boundary component. Note that in each

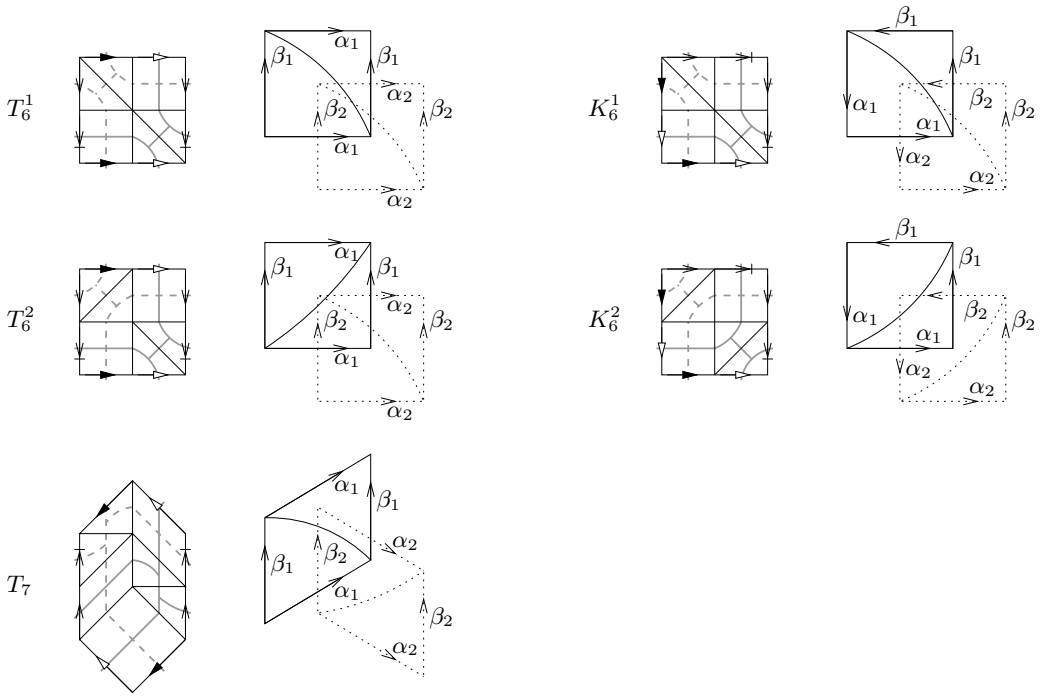

Fig. 20. Representations of the untwisted thin I-bundles T_6^1, T_6^2, T_7, K_6^1 and K_6^2

case α_1 and β_1 generate the fundamental group of the upper boundary surface and α_2 and β_2 generate the fundamental group of the lower boundary surface.

Let p, q, r and s be integers and let θ be one of the thin I-bundles depicted in Figure 20. We define $B_{\theta|p,q|r,s}$ to be the specific layered surface bundle obtained by identifying the upper and lower boundaries of θ so that directed edge α_1 maps to $\alpha_2^p\beta_2^q$ and directed edge β_1 maps to $\alpha_2^r\beta_2^s$.

Note that for some values of p, q, r and s this identification can be realised by an immediate mapping of the corresponding boundary faces. On the other hand, for some values of p, q, r and s an additional layering of tetrahedra is required so that $\alpha_2^p\beta_2^q$, $\alpha_2^r\beta_2^s$ and the corresponding diagonal actually appear as edges of the lower boundary surface.

Note also that for some values of p, q, r and s this construction is not possible since there is no homeomorphism identifying the upper and lower boundaries as required.

Example 3.3 As an illustration of this construction, we present the triangulations $B_{T_7|1,1|1,0}$ and $B_{T_6^2|-1,1|2,-1}$.

The construction of $B_{T_7|1,1|1,0}$ begins with the thin I-bundle T_7, depicted in Figure 22. Our task is to identify the upper and lower boundaries so that α_1 and

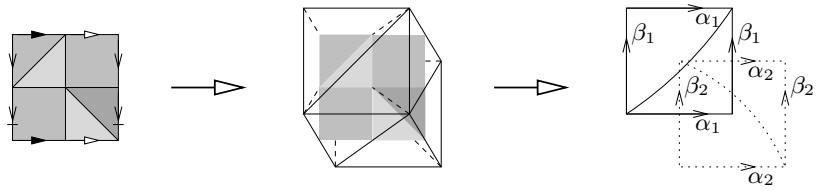

Fig. 21. Relating the central surface decomposition and the boundary for T_6^2

β_1 map to $\alpha_2\beta_2$ and α_2 respectively.

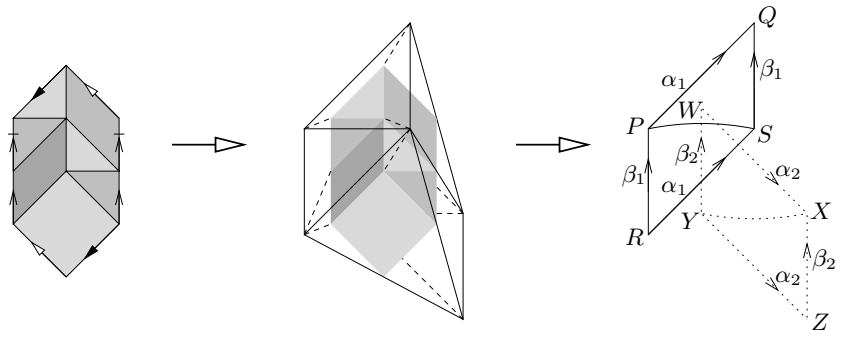

Fig. 22. Constructing the layered surface bundle $B_{T_7|1,1|1,0}$

This can in fact be done using a direct identification, by mapping boundary face RPS to YZX and mapping boundary face PSQ to YWX. The final triangulation $B_{T_7|1,1|1,0}$ therefore has seven tetrahedra, with no additional layering taking place.

The construction of $B_{T_6^2|-1,1|2,-1}$ is slightly more complex. Figure 23 illustrates the thin I-bundle T_6^2. Here we must identify the boundaries so that α_1 and β_1 map to $\alpha_2^{-1}\beta_2$ and $\alpha_2^2\beta_2^{-1}$ respectively. Unfortunately this cannot be done using a direct identification of the boundaries since $\alpha_2^2\beta_2^{-1}$ does not appear as an edge of the lower boundary surface.

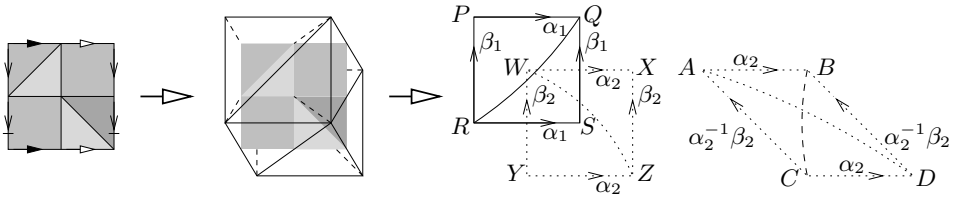

Fig. 23. Constructing the layered surface bundle $B_{T_6^2|-1,1|2,-1}$

We are therefore forced to layer a new tetrahedron onto the lower boundary. This additional tetrahedron, labelled $ABCD$ in the diagram, is layered upon edge XZ so that faces YWZ and CBD are identified and faces WZX and ACB are identified. As a result we obtain a new lower boundary edge AD that indeed represents the curve $\alpha_2^2\beta_2^{-1}$.

We can thus complete the triangulation by identifying the new lower boundary with the original upper boundary, mapping face PQR to DBA and face QRS to DCA. The final triangulation $B_{T_6^2|-1,1|2,-1}$ has seven tetrahedra.

For any layered surface bundle of a form described in Definition 3.2, the underlying 3-manifold can be identified using the following result.

Theorem 3.4 For each set of integers p, q, r and s for which the corresponding triangulations can be constructed, the underlying 3-manifolds of the layered surface bundles with parameters p, q, r and s are as follows.

- $B_{T_6^1|p,q|r,s}$ and $B_{T_6^2|p,q|r,s}$ are both triangulations of the space $T^2 \times I/\left[\begin{smallmatrix} p & r \\ q & s \end{smallmatrix}\right]$.
- $B_{T_7|p,q|r,s}$ is a triangulation of the space $T^2 \times I/\left[\begin{smallmatrix} (p+q) & (r+s) \\ q & s \end{smallmatrix}\right]$.
- Assume that $p + r$ is odd, $|p - q| = |r - s| = 1$ and $p - q + r - s = 0$. Then triangulations $B_{K_6^1|p,q|r,s}$ and $B_{K_6^2|p,q|r,s}$ both represent the space $K^2 \times I/\left[\begin{smallmatrix} (\{p\}-\{r\}) & \{r\} \\ 0 & (s-r) \end{smallmatrix}\right]$, where the symbol $\{x\}$ is defined to be 1 if x is odd and 0 if x is even.

Proof It can be observed from Figure 20 that α_2 is parallel to α_1 and β_2 is parallel to β_1 within each of the I-bundles T_6^1, T_6^2, K_6^1 and K_6^2. Within the I-bundle T_7 we find that α_2 is parallel to α_1 and that β_2 is parallel to $\alpha_1\beta_1$.

Given these observations, it is a simple matter to convert the identification of the two boundary surfaces into the canonical form described in Section 3.1 and thus establish the above results. □

3.3. *Plugged Thin I-Bundles*

Plugged thin I-bundles are formed by attaching layered solid tori to twisted I-bundles over the torus. The resulting 3-manifolds are all Seifert fibred, where we allow Seifert fibred spaces over orbifolds as well as over surfaces. Details of the construction are as follows.

Definition 3.5 (Plugged Thin I-Bundle) A *plugged thin I-bundle* is a 3-manifold triangulation formed using the following construction. Begin with one of the thin I-bundles over the torus depicted in Figure 24. Note from the markings on the diagrams that each I-bundle is twisted and non-orientable, specifically with a twist as we wrap from top to bottom in each diagram and no twist as we wrap from left

to right. An example of the full enclosing triangulation for the case $\tilde{T}_6^2$ can be see in Figure 25.

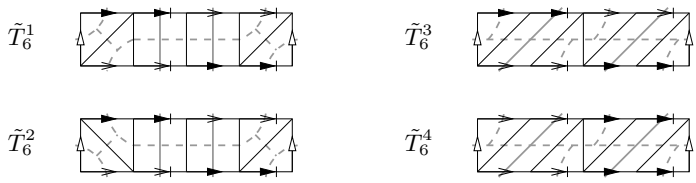

Fig. 24. Representations of the twisted thin I-bundles $\tilde{T}_6^1$, $\tilde{T}_6^2$, $\tilde{T}_6^3$ and $\tilde{T}_6^4$

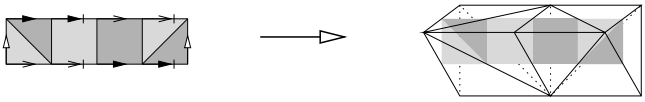

Fig. 25. The full twisted thin I-bundle $\tilde{T}_6^2$

Each thin I-bundle has a single boundary with four faces, and each of these boundaries forms a torus as illustrated in Figure 26. We observe that each of these torus boundaries is formed from two annuli, one on the left and one on the right. Our construction is then completed by attaching a layered solid torus to each of these annuli as illustrated in Figure 27.

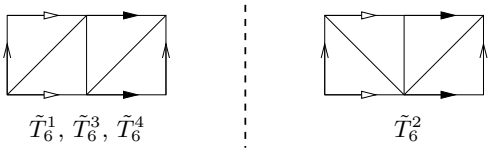

Fig. 26. The possible torus boundaries of thin I-bundles $\tilde{T}_6^1$, $\tilde{T}_6^2$, $\tilde{T}_6^3$ and $\tilde{T}_6^4$

Let the layered solid tori have parameters $\mathrm{LST}(p_1, q_1, r_1)$ and $\mathrm{LST}(p_2, q_2, r_2)$ as explained in Definition 2.11. Furthermore, let the layered solid torus edges with parameters p_i be attached to the left and right edges of the I-bundle boundary and let the layered solid torus edges with parameters q_i be attached to the top and bottom edges of the I-bundle boundary as shown in Figure 27. Then the particular plugged thin I-bundle that has been constructed is denoted $H_{\theta|p_1,q_1|p_2,q_2}$, where θ denotes the original thin I-bundle chosen from Figure 24.

Note that instead of attaching a standard layered solid torus, the two faces of an annulus may be identified with each other by attaching the 0-tetrahedron degenerate $\mathrm{LST}(2, -1, -1)$, i.e., a Möbius band. For brevity, if a pair p_i, q_i is omitted from the

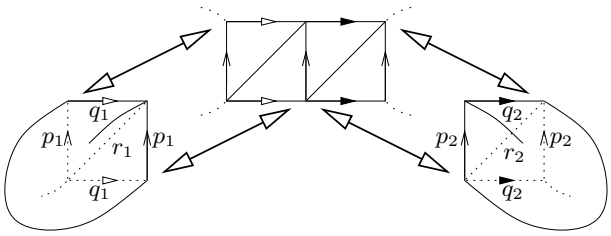

Fig. 27. Attaching layered solid tori to the torus boundary

symbolic name of a plugged thin I-bundle then this pair is assumed to be $2, -1$. For instance, the plugged thin I-bundle $H_{\tilde{T}_6^2|3,-1}$ is in fact $H_{\tilde{T}_6^2|3,-1|2,-1}$.

Note also that the triangulations $H_{\theta|p_1,q_1|p_2,q_2}$ and $H_{\theta|p_2,q_2|p_1,q_1}$ are isomorphic. This can be seen from the symmetries of the layered solid torus and of the thin I-bundles described in Figure 24.

The following result allows us to identify the underlying 3-manifold of a plugged thin I-bundle.

Theorem 3.6 Let p_1 and q_1 be coprime integers and let p_2 and q_2 be coprime integers, where $p_1 \neq 0$ and $p_2 \neq 0$. Then the underlying 3-manifolds of the plugged thin I-bundles with parameters p_1, q_1, p_2 and q_2 are as follows.[1]

- $H_{\tilde{T}_6^1|p_1,q_1|p_2,q_2}$, $H_{\tilde{T}_6^2|p_1,q_1|p_2,q_2}$ and $H_{\tilde{T}_6^3|p_1,q_1|p_2,q_2}$ are each triangulations of the Seifert fibred space $\mathrm{SFS}\big(\mathbb{R}P^2 : (p_1, q_1),\ (p_2, p_2 + q_2)\big)$.
- $H_{\tilde{T}_6^4|p_1,q_1|p_2,q_2}$ is a triangulation of the Seifert fibred space $\mathrm{SFS}\big(\bar{D} : (p_1, q_1),\ (p_2, q_2)\big)$, where the orbifold $\bar{D}$ is a disc with reflector boundary.

Proof Consider the boundary torus of each of the thin I-bundles $\tilde{T}_6^1$, $\tilde{T}_6^2$, $\tilde{T}_6^3$ and $\tilde{T}_6^4$ as seen in Figure 26. We fill each of these boundary tori with circular fibres running parallel to the left and right sides as illustrated in Figure 28.

Fig. 28. Circular fibres on the boundary tori of thin I-bundles

[1]In a previous version of this paper, the first 3-manifold was incorrectly given as the space $\mathrm{SFS}\big(\mathbb{R}P^2 : (p_1, q_1),\ (p_2, q_2)\big)$.

Our aim is to find compatible fibrations of the thin I-bundles. Each of the I-bundles $\tilde{T}_6^1$, $\tilde{T}_6^2$ and $\tilde{T}_6^3$ can be realised as a trivial Seifert fibred space over the Möbius band. The I-bundle $\tilde{T}_6^4$ on the other hand can be realised as a trivial Seifert fibred space over an orbifold, where this base orbifold is an annulus with one reflector boundary. In all cases the fibration of the I-bundle is compatible with the fibration of the boundary torus.

Attaching our two layered solid tori completes the fibrations, filling each base space with a disc and introducing exceptional fibres with parameters (p_1, q_1) and $(p_2, p_2 + q_2)$. After normalising the Seifert invariants, the resulting 3-manifolds can be expressed as $\mathrm{SFS}\left(\mathbb{R}P^2 : (p_1, q_1),\ (p_2, p_2 + q_2)\right)$ and $\mathrm{SFS}\left(\bar{D} : (p_1, q_1),\ (p_2, q_2)\right)$ as claimed. □

3.4. *Plugged Thick I-Bundles*

Plugged thick I-bundles are similar to the plugged thin I-bundles of Section 3.3, except that instead of attaching layered solid tori directly to thin I-bundles we first wrap the thin I-bundles with an additional padding of tetrahedra. As with plugged thin I-bundles, the resulting 3-manifolds are all Seifert fibred.

We begin by presenting four triangulations of a twisted I-bundle over the torus, each of which has two vertices on the boundary.

Definition 3.7 (Two-Vertex I-Bundles $\tilde{T}_5^1, \ldots, \tilde{T}_5^4$) Let $\tilde{T}_3^1$, $\tilde{T}_3^2$ and $\tilde{T}_5^1$ be the thin I-bundles over the torus depicted in Figure 29. Note that $\tilde{T}_3^1$ and $\tilde{T}_3^2$ are in fact the same triangulation presented in different ways. From the markings we see that each I-bundle is twisted and non-orientable, specifically with a twist as we wrap from top to bottom and no twist as we wrap from left to right. The boundary torus of each I-bundle is illustrated alongside each diagram. The full enclosing triangulation for the case $\tilde{T}_5^1$ is illustrated in Figure 30.

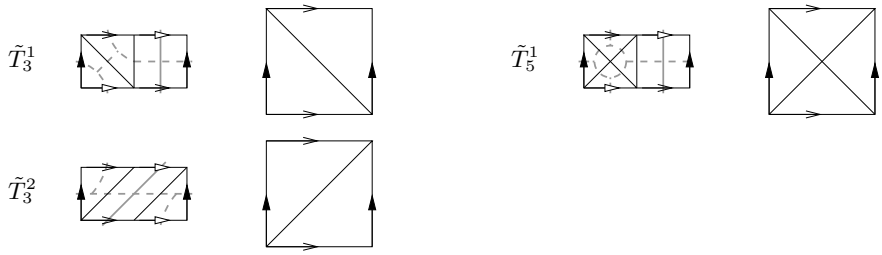

Fig. 29. Representations of the twisted thin I-bundles $\tilde{T}_3^1$, $\tilde{T}_3^2$ and $\tilde{T}_5^1$

We see that $\tilde{T}_5^1$ already has two boundary vertices. For $\tilde{T}_3^1$ and $\tilde{T}_3^2$ we modify the boundary by attaching a square pyramid formed from two tetrahedra. The apex of this pyramid becomes the second boundary vertex.

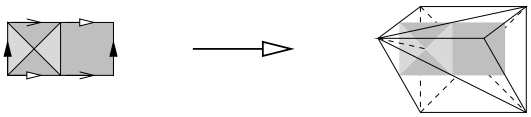

Fig. 30. The full twisted thin I-bundle $\tilde{T}_5^1$

Figure 31 shows three new I-bundles $\tilde{T}_5^2$, $\tilde{T}_5^3$ and $\tilde{T}_5^4$ obtained in this fashion. To construct $\tilde{T}_5^2$ and $\tilde{T}_5^3$ we attach a pyramid to the boundary of $\tilde{T}_3^1$; triangulation $\tilde{T}_5^3$ differs in that the base of the pyramid wraps around the upper and lower edges of the diagram. To construct $\tilde{T}_5^4$ we attach a pyramid to the boundary of $\tilde{T}_3^2$. The new two-vertex boundary tori are depicted on the right hand side of Figure 31.

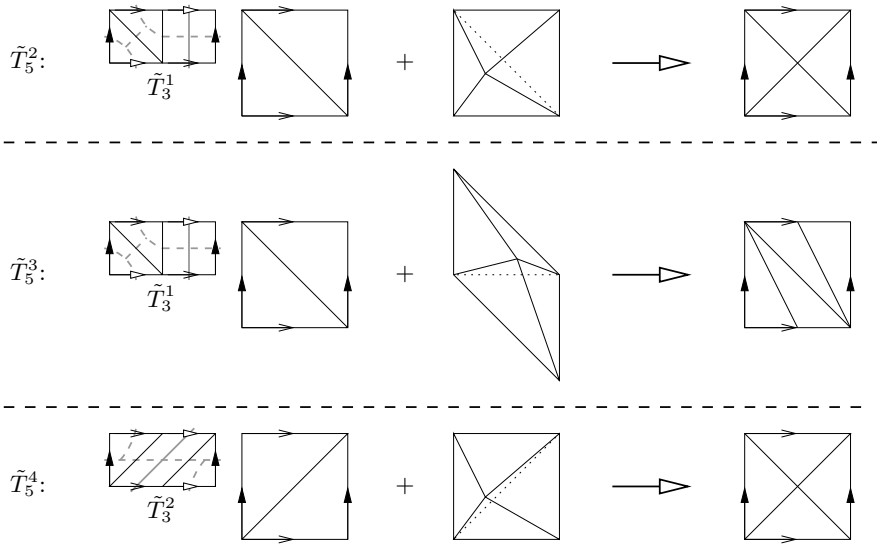

Fig. 31. Constructing twisted I-bundles $\tilde{T}_5^2$, $\tilde{T}_5^3$ and $\tilde{T}_5^4$

We see then that each of the I-bundles $\tilde{T}_5^1$, $\tilde{T}_5^2$, $\tilde{T}_5^3$ and $\tilde{T}_5^4$ is formed from five tetrahedra and has a two-vertex torus boundary.

Having constructed the I-bundles $\tilde{T}_5^1$, $\tilde{T}_5^2$, $\tilde{T}_5^3$ and $\tilde{T}_5^4$, we proceed to define a plugged thick I-bundle as follows.

Definition 3.8 (Plugged Thick I-Bundle) A *plugged thick I-bundle* is a 3-manifold triangulation formed using the following construction. Beginning with one of the two-vertex twisted I-bundles $\tilde{T}_5^1$, $\tilde{T}_5^2$, $\tilde{T}_5^3$ or $\tilde{T}_5^4$, we layer a single tetrahedron onto a specific edge of the boundary torus. This layering must form a new boundary

edge running vertically from top to bottom; Figure 32 shows where this layering occurs for each of the I-bundles $\tilde{T}_5^1$, $\tilde{T}_5^2$, $\tilde{T}_5^3$ and $\tilde{T}_5^4$.

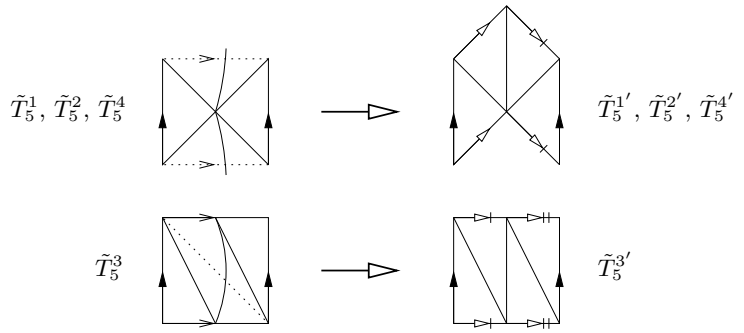

Fig. 32. Layering a tetrahedron to form twisted I-bundles $\tilde{T}_5^{1'}$, $\tilde{T}_5^{2'}$, $\tilde{T}_5^{3'}$ and $\tilde{T}_5^{4'}$

Specifically, for $\tilde{T}_5^1$, $\tilde{T}_5^2$ and $\tilde{T}_5^4$ the new tetrahedron is layered upon the top and bottom edges of the diagram. For $\tilde{T}_5^3$ the new tetrahedron is layered upon the main diagonal. The resulting I-bundles are labelled $\tilde{T}_5^{1'}$, $\tilde{T}_5^{2'}$, $\tilde{T}_5^{3'}$ and $\tilde{T}_5^{4'}$ respectively, and their new torus boundaries are shown on the right hand side of Figure 32.

At last we find ourselves in familiar territory. The boundary tori of the new six-tetrahedron I-bundles $\tilde{T}_5^{1'}$, $\tilde{T}_5^{2'}$, $\tilde{T}_5^{3'}$ and $\tilde{T}_5^{4'}$ are each formed from two annuli, one on the left and one on the right. As with the plugged thin I-bundles of the previous section, we complete the construction by attaching a layered solid torus to each annulus as illustrated in Figure 33.

Let the layered solid tori have parameters $\mathrm{LST}(p_1, q_1, r_1)$ and $\mathrm{LST}(p_2, q_2, r_2)$, where the edges with parameters p_i are attached to the left and right edges of the I-bundle boundary and where the edges with parameters q_i are attached to the top and bottom edges of the I-bundle boundary. Let θ be $\tilde{T}_5^1$, $\tilde{T}_5^2$, $\tilde{T}_5^3$ or $\tilde{T}_5^4$ according to which of the two-vertex twisted I-bundles was selected at the the beginning of the construction. Then the specific plugged thick I-bundle that has been constructed is denoted $K_{\theta|p_1,q_1|p_2,q_2}$.

Again the two faces of an annulus may instead be identified with each other by attaching the degenerate $\mathrm{LST}(2, -1, -1)$, i.e., a Möbius band. If a pair p_i, q_i is omitted from the symbolic name of a plugged thick I-bundle then this pair is once more assumed to be $2, -1$. As an example, the plugged thick I-bundle $K_{\tilde{T}_5^3|3,-1}$ is in reality $K_{\tilde{T}_5^3|3,-1|2,-1}$.

The identification of the underlying 3-manifold of a plugged thick I-bundle is similar to that for a plugged thin I-bundle, as seen in the following result.

Theorem 3.9 Let p_1 and q_1 be coprime integers and let p_2 and q_2 be coprime integers, where $p_1 \neq 0$ and $p_2 \neq 0$. Then the underlying 3-manifolds of the plugged

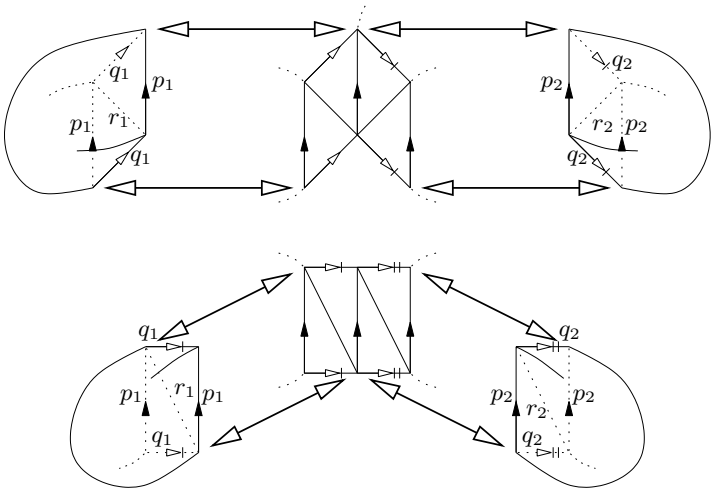

Fig. 33. Attaching layered solid tori to the torus boundary

thick I-bundles with parameters p_1, q_1, p_2 and q_2 are as follows.[2]

- $K_{\tilde{T}_5^1|p_1,q_1|p_2,q_2}$, $K_{\tilde{T}_5^2|p_1,q_1|p_2,q_2}$ and $K_{\tilde{T}_5^3|p_1,q_1|p_2,q_2}$ are each triangulations of the Seifert fibred space $\mathrm{SFS}\big(\mathbb{R}P^2 : (p_1,q_1),\ (p_2,p_2+q_2)\big)$.
- $K_{\tilde{T}_5^4|p_1,q_1|p_2,q_2}$ is a triangulation of the Seifert fibred space $\mathrm{SFS}\big(\bar{D} : (p_1,q_1),\ (p_2,-q_2)\big)$, where the orbifold $\bar{D}$ is a disc with reflector boundary.

Proof The proof is almost identical to the proof of Theorem 3.6. Once more we fill the boundary tori of $\tilde{T}_5^{1'}$, $\tilde{T}_5^{2'}$, $\tilde{T}_5^{3'}$ and $\tilde{T}_5^{4'}$ with circular fibres that run parallel to the left and right sides as illustrated in Figure 34.

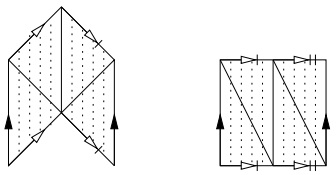

Fig. 34. Circular fibres on the boundary tori of thick I-bundles

Compatible fibrations of the interior I-bundles and the exterior layered solid tori are found as before, resulting in the 3-manifolds listed above. □

[2]In a previous version of this paper, these 3-manifolds were incorrectly given as the spaces $\mathrm{SFS}\big(\mathbb{R}P^2 : (p_1,q_1),\ (p_2,q_2)\big)$ and $\mathrm{SFS}\big(\bar{D} : (p_1,q_1),\ (p_2,q_2)\big)$.

3.5. *Exceptional Triangulations*

Three triangulations appear in the ≤ 7-tetrahedron non-orientable census that do not fit neatly into any of the families described thus far. Each of these triangulations consists of precisely six tetrahedra and is formed using a variant of a previous construction. Specific details of these three triangulations are as follows.

Definition 3.10 (Triangulations $E_{6,1}$ and $E_{6,2}$) Triangulations $E_{6,1}$ and $E_{6,2}$ use a construction similar to the plugged thin I-bundles discussed in Section 3.3. Let $\tilde{T}_6^1$ and $\tilde{T}_6^2$ be the thin I-bundles over the torus depicted in the upper section of Figure 35 (these are the same $\tilde{T}_6^1$ and $\tilde{T}_6^2$ as used in Definition 3.5). Each of these thin I-bundles has a torus boundary, illustrated in the lower portion of the figure. Triangulations $E_{6,1}$ and $E_{6,2}$ are formed from $\tilde{T}_6^1$ and $\tilde{T}_6^2$ respectively by identifying the faces of their torus boundaries as follows.

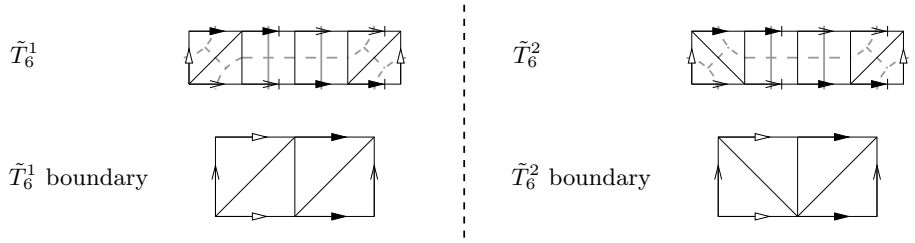

Fig. 35. Representations of the thin I-bundles used in the construction of $E_{6,1}$ and $E_{6,2}$

Figure 36 illustrates the construction of $E_{6,1}$. Beginning with $\tilde{T}_6^1$, we identify the boundary face ADB with EBC and we identify the boundary face DBE with EFC. The resulting edge identifications are shown on the right hand side of the diagram.

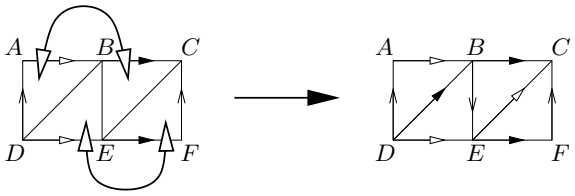

Fig. 36. Constructing exceptional triangulation $E_{6,1}$

The construction of $E_{6,2}$ is illustrated in Figure 37. This time we begin with $\tilde{T}_6^2$, identifying the boundary face AEB with ECF and identifying the boundary face DAE with BEC. Again the resulting edge identifications are shown.

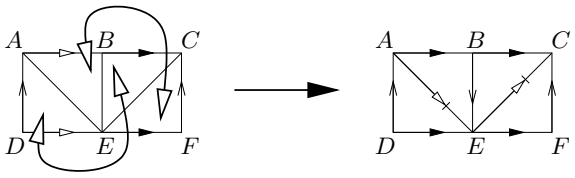

Fig. 37. Constructing exceptional triangulation $E_{6,2}$

Definition 3.11 (Triangulation $E_{6,3}$) Triangulation $E_{6,3}$ is formed from a pair of three-tetrahedron thin I-bundles as follows. Let $\tilde{T}_3^1$ be the thin I-bundle over the torus depicted in Figure 38 (this is the same $\tilde{T}_3^1$ as used in Definition 3.7). This thin I-bundle has a torus boundary as shown in the right hand portion of the diagram.

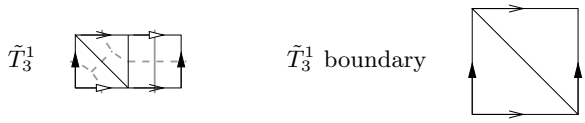

Fig. 38. A representation of the thin I-bundle used in the construction of $E_{6,3}$

The construction of $E_{6,3}$ involves taking two copies of $\tilde{T}_3^1$ and identifying their boundary tori according to a particular homeomorphism. This identification is illustrated in Figure 39. Specifically, face ABD is identified with XZW and face ACD is identified with ZWY. The resulting edge identifications are shown in the diagram.

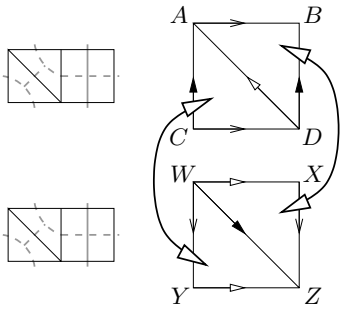

Fig. 39. Constructing exceptional triangulation $E_{6,3}$

Each of the exceptional triangulations $E_{6,1}$, $E_{6,2}$ and $E_{6,3}$ can be converted using Pachner moves [16] into a layered surface bundle, at which point the underlying 3-manifold can be identified using Theorem 3.4. A list of the resulting 3-manifolds

can be found in Section 4.2.

4. Census Results

We conclude with a presentation of all closed non-orientable minimal $\mathbb{P}^2$-irreducible triangulations formed from at most seven tetrahedra. Recall from Section 1 that this list contains 41 distinct triangulations, together representing just eight different 3-manifolds.

Section 4.1 lists these 41 triangulations according to method of construction and Section 4.2 groups them according to their underlying 3-manifolds. Note that almost all of the 3-manifolds found in the census allow for more than one minimal triangulation. In such cases every minimal triangulation is presented.

A *Regina* data file containing all of the census triangulations listed here can be downloaded from the *Regina* website [3].

4.1. *Triangulations*

We present here the 41 census triangulations ordered first by number of tetrahedra and then by method of construction. Table 2 shows how these 41 triangulations are distributed amongst the different families described in Section 3. Note that the figures in the six-tetrahedron column sum to 25 whereas the total is listed as 24; this is because one of the six-tetrahedron triangulations can be viewed as both a layered torus bundle and a layered Klein bottle bundle.

Table 2. Frequencies of triangulations from different families

Tetrahedra	1–5	6	7	**Total**
Layered torus bundles	0	6	4	10
Layered Klein bottle bundles	0	8	0	8
Plugged thin I-bundles	0	4	6	10
Plugged thick I-bundles	0	4	7	11
Exceptional triangulations	0	3	0	3
Total	0	24	17	41

Since there are no closed non-orientable minimal $\mathbb{P}^2$-irreducible triangulations formed from five tetrahedra or fewer, we use six tetrahedra as the starting point for our detailed enumeration.

4.1.1. *Six Tetrahedra*

The six-tetrahedron closed non-orientable minimal $\mathbb{P}^2$-irreducible triangulations are as follows.

- The layered torus bundles $B_{T_6^1|-1,0|-1,1}$, $B_{T_6^1|0,-1|-1,0}$, $B_{T_6^1|0,1|1,0}$, $B_{T_6^1|1,0|1,-1}$,

$B_{T_6^2|-1,1|1,0}$ and $B_{T_6^2|1,0|0,-1}$ as described by Definition 3.2, where one of these layered torus bundles is isomorphic to a layered Klein bottle bundle as discussed below;

- The layered Klein bottle bundles $B_{K_6^1|-1,0|0,-1}$, $B_{K_6^1|0,-1|-1,0}$, $B_{K_6^1|0,1|1,0}$, $B_{K_6^1|1,0|0,1}$, $B_{K_6^2|-1,0|0,-1}$, $B_{K_6^2|0,-1|-1,0}$, $B_{K_6^2|0,1|1,0}$ and $B_{K_6^2|1,0|0,1}$ as again described by Definition 3.2, where one of these layered Klein bottle bundles is isomorphic to a layered torus bundle as discussed below;
- The plugged thin I-bundles $H_{\tilde{T}_6^1}$, $H_{\tilde{T}_6^2}$, $H_{\tilde{T}_6^3}$ and $H_{\tilde{T}_6^4}$ as described by Definition 3.5;
- The plugged thick I-bundles $K_{\tilde{T}_5^1}$, $K_{\tilde{T}_5^2}$, $K_{\tilde{T}_5^3}$ and $K_{\tilde{T}_5^4}$ as described by Definition 3.8;
- The exceptional triangulations $E_{6,1}$, $E_{6,2}$ and $E_{6,3}$ as described in Section 3.5.

Although 25 triangulations are named above, two of these are isomorphic. More specifically, the layered torus bundle $B_{T_6^1|0,1|1,0}$ is isomorphic to the layered Klein bottle bundle $B_{K_6^2|0,-1|-1,0}$, leaving 24 distinct triangulations in our list.

4.1.2. *Seven Tetrahedra*

The seven-tetrahedron closed non-orientable minimal $\mathbb{P}^2$-irreducible triangulations are as follows.

- The layered torus bundles $B_{T_6^2|-1,1|2,-1}$, $B_{T_6^2|0,-1|-1,2}$, $B_{T_7|-1,-1|-1,0}$ and $B_{T_7|1,1|1,0}$ as described by Definition 3.1;
- The plugged thin I-bundles $H_{\tilde{T}_6^1|3,-2}$, $H_{\tilde{T}_6^1|3,-1}$, $H_{\tilde{T}_6^2|3,-2}$, $H_{\tilde{T}_6^2|3,-1}$, $H_{\tilde{T}_6^3|3,-1}$ and $H_{\tilde{T}_6^4|3,-1}$ as described by Definition 3.5;
- The plugged thick I-bundles $K_{\tilde{T}_5^1|3,-1}$, $K_{\tilde{T}_5^2|3,-2}$, $K_{\tilde{T}_5^2|3,-1}$, $K_{\tilde{T}_5^3|3,-2}$, $K_{\tilde{T}_5^3|3,-1}$, $K_{\tilde{T}_5^4|3,-2}$ and $K_{\tilde{T}_5^4|3,-1}$ as described by Definition 3.8.

4.2. *3-Manifolds*

We close with a table of all closed non-orientable $\mathbb{P}^2$-irreducible 3-manifolds formed from seven tetrahedra or fewer. These 3-manifolds are listed in Table 3, along with their first homology groups and minimal triangulations. Recall from Section 3 that the orbifold $\bar{D}$ is a disc with reflector boundary.

Acknowledgements

The author would like to thank the Australian Research Council and the University of Melbourne for supporting this research, much of which was funded under ARC project DP0208490.

Table 3. All eight 3-manifolds and their 41 minimal triangulations

Δ	**3-Manifold**	**Triangulations**	**Homology**
6	$T^2 \times I/\left[\begin{smallmatrix}-1 & 1\\ 1 & 0\end{smallmatrix}\right]$	$B_{T_6^2\|-1,1\|1,0}$	$\mathbb{Z}$
	$T^2 \times I/\left[\begin{smallmatrix}0 & 1\\ 1 & 0\end{smallmatrix}\right]$	$B_{T_6^1\|-1,0\|-1,1}$, $B_{T_6^1\|0,-1\|-1,0}$, $(B_{T_6^1\|0,1\|1,0} = B_{K_6^2\|0,-1\|-1,0})$, $B_{T_6^1\|1,0\|1,-1}$, $B_{K_6^1\|0,-1\|-1,0}$, $E_{6,3}$	$\mathbb{Z} \oplus \mathbb{Z}$
	$K^2 \times S^1$	$B_{T_6^2\|1,0\|0,-1}$, $B_{K_6^1\|1,0\|0,1}$, $B_{K_6^2\|1,0\|0,1}$	$\mathbb{Z} \oplus \mathbb{Z} \oplus \mathbb{Z}_2$
	$K^2 \times I/\left[\begin{smallmatrix}-1 & 1\\ 0 & -1\end{smallmatrix}\right]$	$B_{K_6^1\|0,1\|1,0}$, $B_{K_6^2\|0,1\|1,0}$, $H_{\tilde{T}_6^1}$, $H_{\tilde{T}_6^2}$, $H_{\tilde{T}_6^3}$, $K_{\tilde{T}_5^1}$, $K_{\tilde{T}_5^2}$, $K_{\tilde{T}_5^3}$, $E_{6,2}$	$\mathbb{Z} \oplus \mathbb{Z}_4$
	$K^2 \times I/\left[\begin{smallmatrix}1 & 0\\ 0 & -1\end{smallmatrix}\right]$	$B_{K_6^1\|-1,0\|0,-1}$, $B_{K_6^2\|-1,0\|0,-1}$, $H_{\tilde{T}_6^4}$, $K_{\tilde{T}_5^4}$, $E_{6,1}$	$\mathbb{Z} \oplus \mathbb{Z}_2 \oplus \mathbb{Z}_2$
7	$T^2 \times I/\left[\begin{smallmatrix}2 & 1\\ 1 & 0\end{smallmatrix}\right]$	$B_{T_6^2\|-1,1\|2,-1}$, $B_{T_6^2\|0,-1\|-1,2}$, $B_{T_7\|-1,-1\|-1,0}$, $B_{T_7\|1,1\|1,0}$	$\mathbb{Z} \oplus \mathbb{Z}_2$
	$\mathrm{SFS}\left(\mathbb{R}P^2 : (2,1)\ (3,1)\right)$	$H_{\tilde{T}_6^1\|3,-2}$, $H_{\tilde{T}_6^1\|3,-1}$, $H_{\tilde{T}_6^2\|3,-2}$, $H_{\tilde{T}_6^2\|3,-1}$, $H_{\tilde{T}_6^3\|3,-1}$, $K_{\tilde{T}_5^1\|3,-1}$, $K_{\tilde{T}_5^2\|3,-2}$, $K_{\tilde{T}_5^2\|3,-1}$, $K_{\tilde{T}_5^3\|3,-2}$, $K_{\tilde{T}_5^3\|3,-1}$	$\mathbb{Z}$
	$\mathrm{SFS}\left(\bar{D} : (2,1)\ (3,1)\right)$	$H_{\tilde{T}_6^4\|3,-1}$, $K_{\tilde{T}_5^4\|3,-2}$, $K_{\tilde{T}_5^4\|3,-1}$	$\mathbb{Z} \oplus \mathbb{Z}_2$

References

[1] Gennaro Amendola and Bruno Martelli, *Non-orientable 3-manifolds of small complexity*, Topology Appl. **133** (2003), no. 2, 157–178.

[2] ———, *Non-orientable 3-manifolds of complexity up to 7*, Topology Appl. **150** (2005), no. 1-3, 179–195.

[3] Benjamin A. Burton, *Regina: Normal surface and 3-manifold topology software*, `http://regina.sourceforge.net/`, 1999–2005.

[4] ———, *Minimal triangulations and normal surfaces*, Ph.D. thesis, University of Melbourne, 2003, available from `http://regina.sourceforge.net/`.

[5] ———, *Face pairing graphs and 3-manifold enumeration*, J. Knot Theory Ramifications **13** (2004), no. 8, 1057–1101.

[6] ———, *Introducing Regina, the 3-manifold topology software*, Experiment. Math. **13** (2004), no. 3, 267–272.

[7] Patrick J. Callahan, Martin V. Hildebrand, and Jeffrey R. Weeks, *A census of cusped*

hyperbolic 3-manifolds, Math. Comp. **68** (1999), no. 225, 321–332.

[8] John Hempel, *3-manifolds*, Annals of Mathematics Studies, no. 86, Princeton University Press, Princeton, NJ, 1976.

[9] Martin V. Hildebrand and Jeffrey R. Weeks, *A computer generated census of cusped hyperbolic 3-manifolds*, Computers and Mathematics (Cambridge, MA, 1989), Springer, New York, 1989, pp. 53–59.

[10] William Jaco and J. Hyam Rubinstein, *0-efficient triangulations of 3-manifolds*, J. Differential Geom. **65** (2003), no. 1, 61–168.

[11] ———, *Layered-triangulations of 3-manifolds*, Preprint, `arXiv:math/0603601`, March 2006.

[12] Bruno Martelli, *Complexity of 3-manifolds*, Spaces of Kleinian Groups, London Math. Soc. Lecture Note Ser., vol. 329, Cambridge Univ. Press, Cambridge, 2006, pp. 91–120.

[13] Bruno Martelli and Carlo Petronio, *Three-manifolds having complexity at most 9*, Experiment. Math. **10** (2001), no. 2, 207–236.

[14] ———, *Complexity of geometric three-manifolds*, Geom. Dedicata **108** (2004), no. 1, 15–69.

[15] Sergei V. Matveev, *Tables of 3-manifolds up to complexity 6*, Max-Planck-Institut für Mathematik Preprint Series (1998), no. 67, available from `http://www.mpim-bonn.mpg.de/html/preprints/preprints.html`.

[16] Udo Pachner, *P.L. homeomorphic manifolds are equivalent by elementary shellings*, European J. Combin. **12** (1991), no. 2, 129–145.

[17] Vladimir G. Turaev and Oleg Y. Viro, *State sum invariants of* 3*-manifolds and quantum* $6j$*-symbols*, Topology **31** (1992), no. 4, 865–902.